www.vbripress.com/aml, DOI: 10.5185/amlett.2016.6155 Published online by the VBRI Press in 2016

Tunable structural, optical and electrical properties of annealed ZnO-SnO_2 composite thin films deposited by pulsed laser deposition

Sudip. K. Sinha*

Department of Metallurgical Engineering, National Institute of Technology Raipur 492010, India

*Corresponding author. Tel: (+91) 9830076244; E-mail: sksinha.met@nitrr.ac.in

Received: 10 September 2015, Revised: 30 November 2015 and Accepted: 03 January 2016

ABSTRACT

We report the thermal annealing effect of ZnO-SnO_2 composite thin films deposited by pulsed laser deposition on its structural, electrical, and optical properties. The results present a consistent portrayal of the evolution of ZnO-SnO_2 composite oxide films phase formation in post-annealed condition and its subsequent effect on various physical properties. X-ray diffraction confirms that the films transform from nearly amorphous to fully crystalline state on thermal annealing at 600 °C. X-ray photoelectron spectroscopy reveals a small shift in Sn-3*d* peak towards lower energy and O-1*s* and Zn-2*p* peaks towards higher binding energy with increasing ZnO concentration and confirms the formation of combined oxides of ZnO and SnO_2. The average optical transmission is greater than 80 % in the visible region of the annealed ZnO-SnO_2 composite films. The lowest electrical resistivity of 9.8×10^{-4} Ωcm has been obtained in the film containing 25 wt % ZnO. Our results suggest that annealed ZnO-SnO_2 composite films with improved electrical and optical properties could find potential use in thin film solar cells or touch pad control panels. Copyright © 2016 VBRI Press.

Keywords: X-ray diffraction; crystalline; electrical; transmission; pulsed laser deposition; photoelectron spectroscopy.

Introduction

In the last few decades, a large number of pristine, doped or composite materials based on zinc and/or tin oxide have been comprehensively studied in various morphologies since they found many interesting uses in photovoltaic applications, catalysis, gas sensing, antistatic coating and transparent conducting oxides as solar electrodes [**1-15**].

Among them, Transparent conducting oxide (TCO) films are widely used in optoelectronic devices such as flat panel displays, thin film transistors, infra-red (IR) reflectors, transparent electrodes and solar cells, because these films possess the desired combinations of high electrical conductivity and good optical transparency [**16-19**]. A vast number of binary compounds such as In_2O_3, ZnO, and SnO_2 have been explored during the last fifty years as potential TCO candidates. Among them, tin-doped In_2O_3, known as indium-tin oxide (ITO) is the most extensively explored material (for flat-panel displays), as it shows room temperature conductivity as high as 13500 S/cm [**20**]. Zinc oxide (ZnO) is an *n*-type, wide band gap (3.37 eV at room temperature) semiconductor with a large exciton energy of 60 meV. However the significant drawback of ZnO is its susceptibility to get corroded under strong acidic and alkaline conditions. On the other hand, pure tin oxide (SnO_2) which is a wide band gap (3.6 eV) semiconductor, does not fulfills the industry standard requirements of transparent conducting electrodes for solar cell fabrication. In an effort to solve this matter, both donor and acceptor doped and/or composite metal oxide semiconductors are thoroughly investigated since decades. It has been found that more efficient donor-dopants (e.g. Al, Ga) improved conductivity as high as 12000 S/cm [**21, 22**]. On the other hand, SnO_2 is the most commonly used TCO as low emissivity coating on architectural glass exhibit conductivities up to 9000 S/cm (when doped with F) [**23**].

Minami *et al.* [**24**] first reported that SnO_2–ZnO binary oxides can combine the advantages of both ZnO and SnO_2. SnO_2–ZnO composite films, in spite of having difficulties in chemical etching, in particular at higher concentration of metallic Sn, might substitute the existing TCO's in certain applications. As both Zn and Sn are more abundant than indium, SnO_2–ZnO composite films can emerge as a low-cost alternative. These two materials have the combined advantage of excellent thermal stability and superior mechanical strength of SnO_2 whiles the greater stability of ZnO under reducing atmosphere. It is worth mentioning that the performance and efficiency of the TCO's depend on various parameters like dopant concentration, deposition conditions and annealing treatment. Previously, many of the TCO thin films have been successfully grown by using Pulsed laser deposition (PLD) technique. It offers numerous benefits as compared to other deposition techniques including precision of thickness, morphology and desired composition of the films grown from of multi-component targets, though uniformity over a large area is a major concern. The substrate

 Copyright © 2016 VBRI Press

temperatures of the PLD films can be relatively lower as compared to other PVD techniques since the kinetic energy (>1 eV) of the ionized and ejected species produced by the laser plasma [**25**] are always higher. In the present contribution, we have explored the structural, optical and electrical properties of annealed SnO_2–ZnO binary films deposited by PLD on *p*-Si (100) and glass substrate with varying ZnO concentration. To the best of our knowledge this is the maiden investigation to exploit PLD to produce annealed SnO_2–ZnO binary thin films for developing TCO coatings or devices.

Materials and Methods

Tin oxide (99.99% pure, Aldrich) and zinc oxide (99.99%) powders in four different mixture blends of were weighed, mixed and rigorously ground in a mortar by manual and /or mechanical means to create a homogeneous distribution of ZnO in SnO_2. The as-prepared powder mixtures were subsequently used to make 1-inch diameter disks by cold pressing through the application of 6 ton load. The green samples were subsequently sintered in air atmosphere at 1000 °C for 4 h. The sintering cycle consists of heating and cooling the samples at the rate of 6 °C per minute in air ambience while holding them isothermally at 1000 °C for 4 h. Borosilicate glass were used as substrates for the films to study the optical transmittance spectra and *p*-Si (100) wafers (resistivity ~ 7-14 Ω-cm) of 10 mm × 10 mm dimensions were used to study structural and electrical characteristics. The substrates were adjusted on a particular substrate holder inside the deposition chamber and positioned parallel to the target. The sample was heated to sustain an isothermal temperature of 500 °C and confirm a uniform film thickness. KrF excimer laser (Lambda Physik COMPEX, wavelength of 248 nm and pulsed duration of 25 ns) was used to deposit the films. The target was continuously rotated during deposition to ensure uniform ablation and avoid denting or drilling.

To deposit high quality and uniform films, the deposition parameters were set as follows: laser energy = 300 mJ, base pressure = 5×10^{-5} mbar, oxygen ambient pressure = 1.1×10^{-1} mbar, substrate temperature = 500 °C, substrate-to-target distance = 45 mm, repetition rate = 10 Hz, laser shots = up to 15000. The as-deposited ZnO-SnO_2 films were then annealed at 600 °C for 1 h in oxygen ambience (2×10^{-1} mbar). Even though the as-deposited films form over a wide range of thickness, only those films with constant film thicknesses (750 ± 25 nm) were chosen to for our measurements. The surface morphology and crystalline quality of the as deposited composite films was investigated by glancing incidence X-ray diffraction (GIXRD), field emission scanning electron microscopy (FESEM) and atomic force microscopy (AFM). Perkin-Elmer Lambda 45 spectrophotometer, in the wavelength range 300–1000 nm was used for recording the optical transmittance spectra. The chemical compositions and bonding states were examined with X-ray photoelectron spectroscopy (ULVAC-PHI, Model PHI 5000 Versa Probe II, Japan) with an Al-K_α X-ray source (1486.6 eV) using a micro focused (100µm, 25 W) beam with a photoelectron takeoff angle of 45°. The main chamber having a base pressure of <1 x 10^{-9} torr was attained by evacuation using turbo-molecular and ion-getter pumps. Photoluminescence (PL) characteristics of as-deposited samples were studied using a He-Cd laser as an excitation source, operating at 325 nm with an output power of 50 mW and a photomultiplier detector. The sheet resistance (R_s) and electrical resistivity (ρ) of the ZnO–SnO_2 thin films were measured by usual four-probe technique at room temperature (~25 °C). To avoid ambiguity and minimize error, resistance of each film was measured at ten different locations on the film surface and the final resistivity was computed by considering the average of the measured values.

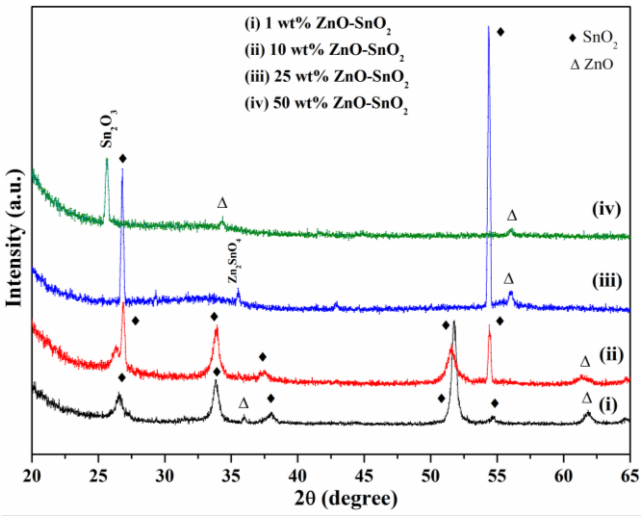

Fig. 1. GIXRD patterns of the ZnO–SnO_2 thin films annealed at 600 °C for 1 h in oxygen atmosphere.

Results and discussion

Fig. 1 shows the GIXRD pattern of the annealed (at 600° C for 1 h at oxygen ambience) ZnO-SnO_2 composite films. The XRD profiles indicate that there is considerable improvement in the film crystallinity [**26**] of the deposited films on annealing, irrespective of their composition. The ZnO-SnO_2 specimens show separate ZnO and SnO_2 peaks at usual Bragg angles, which implies that there is no (or limited) mutual solid solubility in the binary-binary films. However, it is difficult to confirm the extent of solid solubility of ZnO into SnO_2 (if any) only by the XRD measurements. We similarly found no observable change in lattice parameter between undoped SnO_2 and SnO_2 in ZnO-SnO_2 binary blends. Peiteado *et al*. [**27**] by means of a solution-based synthesis route, have earlier shown, that < 0.1 mol% of SnO_2 is soluble in ZnO. It is worth mentioning here that ZnO–SnO_2 phase diagram is not determined or reported till date [**28**]. It is evident from the GIXRD plot that the films crystallinity considerably decreases with the increasing ZnO concentration. Moreover, at higher ZnO concentration of 25 wt % and 50 wt %, Sn_2O_3 phase appears at 2θ = 25.66° and an intermediate cubic spinel compound Zn_2SnO_4 (JCPDF file no. 74-2184) forms, apart from the usual peaks of tetragonal SnO_2 (JCPDF file no. 41-1445) and wurtzite ZnO phases (JCPDF file no. 36-1451), respectively. At

Copyright © 2016 VBRI Press

lower ZnO concentration (1 wt % and 10 wt % ZnO), prominent peaks corresponding to tetragonal SnO_2 (at 2θ = 26.65°, 33.87°, 51.75° and 54.3°) along with the weak peaks of hexagonal ZnO appear (at 35.85° and 61.85°) in the annealed films. In addition, there is another very low intensity weak peak at 26.43° in the 10 wt % ZnO sample which is not accurately identified. No signature of preferential crystal growth in any plane of the deposited or annealed films has been observed.

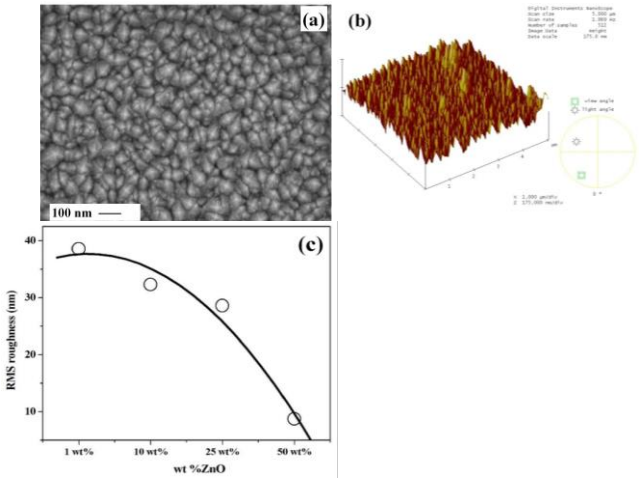

Fig. 2 (a) FESEM image of the 10 wt% ZnO– 90 wt% SnO_2 thin film (b) 3D-AFM image of 10 wt% ZnO–90 wt% SnO_2 thin film (c) Surface roughness (RMS) plot of the ZnO–SnO_2 thin films as a function of increasing ZnO content in the target.

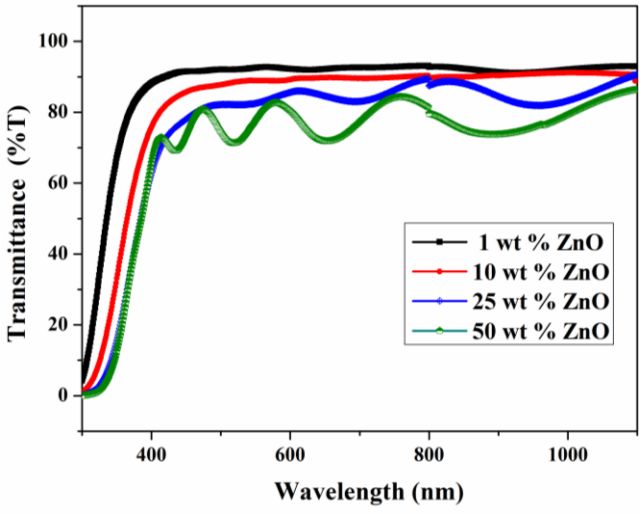

Fig. 3. Optical transmission spectra of the ZnO–SnO_2 thin films with different ZnO concentrations in the target.

The representative microstructural and surface topography of one of the (10 wt % ZnO) SnO_2–ZnO composite films has been presented in **Fig. 2a** (FESEM) and **Fig. 2b** (AFM), respectively. The morphology of the 10 wt % ZnO film shows uniform walnut-like structure with distinct grain boundary distribution. Other films (not shown) reveal similar FESEM morphology with varying grain size. The said morphology revealed by FESEM images correlates well with the GIXRD findings. The surface morphology of the SnO_2–ZnO thin films has been studied by three-dimensional AFM. **Fig. 2(c)** shows the AFM root mean square (RMS) plot of the post-annealed SnO_2–ZnO thin films with varying ZnO concentration ranging from 1.0 wt % to 50 wt %. The mid-region of the as-deposited film was examined which cover an area of 4 μm × 4 μm for measurement. It is evident from the RMS plot that the surface morphology of each sample varies significantly with the amount of ZnO addition. In addition, the RMS roughness decreases nearly in a linear manner with increasing ZnO content (RMS roughness values are 35.6 nm, 32.15 nm, 27.45 nm and 8.62 nm with increasing ZnO concentration of 1 wt %, 10 wt %, 25 wt % and 50 wt % ZnO, respectively). This trend is in agreement with our recently published AFM results, [**26**] that film crystallinity as well as roughness enhances with post-deposition annealing compared to that in the as-deposited (amorphous) state. The optical transmission of the annealed ZnO–SnO_2 films deposited on glass substrates were investigated in the wavelength range 300 to 1100 nm (**Fig. 3**). It appears that optical transmission of the annealed ZnO–SnO_2 films significantly increases as compared to that in the as-deposited ones [**26**], which might be attributed to both better crystallization of the films and lower level of defects near the grain boundaries, thereby resulting in improvement of structural homogeneity and decrease of internal scattering of light.

The film with 50 wt % ZnO shows typical intensity oscillations in the visible region owing to the interference issue in thin films. The absorption edge of the composite films shifts toward higher wavelength range (red shift) with increasing ZnO content, as evident from **Fig. 3**. This change in absorption edge may be ascribed to both compositional change and structural modification of the composite films. The modification in the degree of crystallinity of the composite films is followed by a large to moderate change of the absorption edges to the higher wavelength regime. This result can be accredited to the decrease of extended to localized state transitions resulting from the band tails formed owing to the defect or disorder [**29**].

The optical band gap (E_g) can be calculated from the Tauc equation [**30**] given by

$$\alpha h\nu = A(E_g - h\nu)^n \quad (1)$$

where, A is a constant related to the effective mass associated with the bands and n is a constant which is equal to 0.5 for a direct-gap material and 2.0 for an indirect-gap material, ignoring excitonic effects. The optical data obtained in **Fig. 3** were analyzed using Tauc's equation and plotted as optical band gap as a function of composition in **Fig. 4(a, b)**. Accordingly, the optical band gap values (E_g), calculated as per the extrapolation scheme enumerated in the inset of **Fig. 4**, lie in the range 3.92 -3.46 eV, varying with ZnO concentration. **Fig. 4(a)** clearly suggests that the band gap decreases with increase in ZnO concentration. The observed band gap values for the annealed ZnO-SnO_2 composite films with 1.0 wt %, 10 wt %, 25 wt % and 50 wt % ZnO concentrations are 3.92, 3.69, 3.51, and 3.45 eV, respectively. For comparison, the E_g values of pulsed laser deposited pure SnO_2 and pure ZnO films have also been included here. A representative band gap plot is shown in **Fig. 4(b)** for the sample with

 Copyright © 2016 VBRI Press

1 wt % ZnO-SnO_2 concentration. The relative band levels of the ZnO-SnO_2 composite thin films and the corresponding electron-hole transition is depicted in inset of **Fig. 4 (b)**.

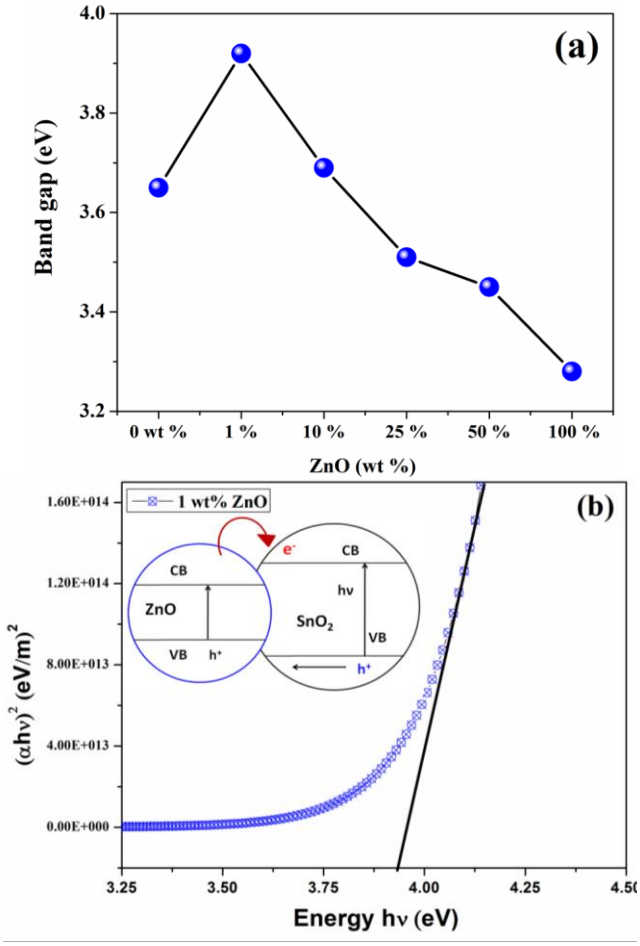

Fig. 4. (a) Optical band gap of the ZnO–SnO_2 thin films with increasing ZnO content. (b) Representative Tauc's plot shows the $(\alpha h\nu)^2$ versus photon energy relation of 1 wt% ZnO sample. Inset shows the electron-hole transition in ZnO-SnO_2 thin film composites.

It is known that in degenerated semiconductors such as SnO_2 and ZnO, the optical band gap can be increased or decreased by varying the carrier concentration. Therefore, the optical band gap value decreases with an increase in ZnO concentration or with the decrease in carrier concentration. It is seen from **Fig. 4** that thermal annealing have increased the band gap of ZnO–SnO_2 composite films with respect to that of the as-deposited ones [**26**]. Earlier Young *et al.* [**31**] have shown that sputter deposited crystalline zinc-tin oxide (ZTO) thin films exhibit a direct optical band gap in the range 3.3 – 3.9 eV. They further concluded that this broad band gap range could probably arise with the combined effect of a large Burstein–Moss (B-M) shift and compositional as well as structural dissimilarity of the zinc-tin oxide thin films.

To further study the effect of ZnO addition to SnO_2 on chemical bonding and structural states of the annealed ZnO–SnO_2 films, XPS study has been carried out for the present set of ZnO–SnO_2 composite films and compared with that for pure SnO_2 film using C-1*s* peak (284.6 eV) as a reference for calibration of binding energy.

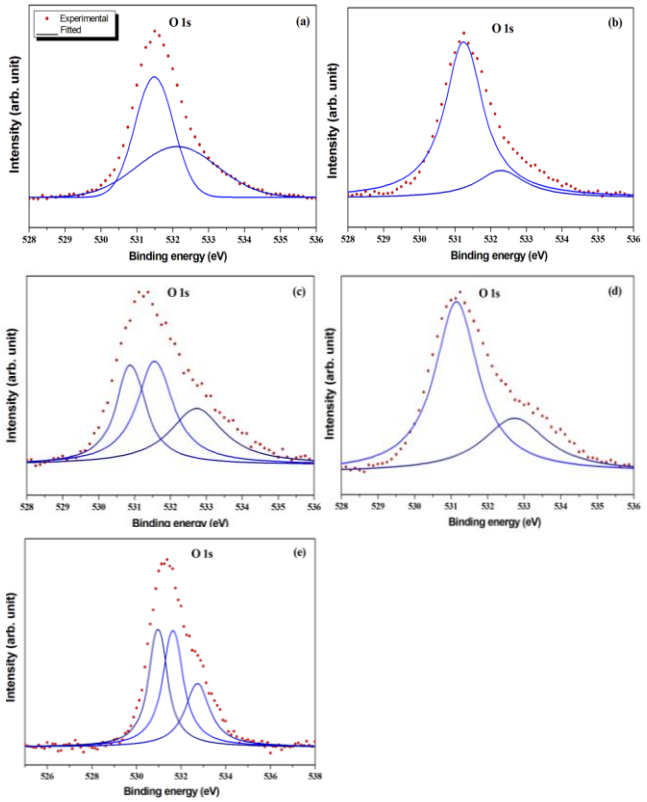

Fig. 5. Peak fitting results of XPS O1s core level spectra of ZnO–SnO_2 thin films with varying ZnO concentration (ZnO:SnO_2 = (a) 0:100 (b) 1:99 (c) 10:90, (d) 25:75 (e) 50:50 wt.%).

The effect of oxidation behavior of the post-annealed ZnO–SnO_2 composite thin films has been well understood by deconvoluting the O-1*s* peaks by two nearly Gaussian curves centered at 531.2 ± 0.2 and 532.5 ± 0.2 eV, as depicted in **Fig. 5(a-e)**. The O-1*s* peak in the ZnO-SnO_2 composite films has been observed in the binding energy region of 531–534 eV. The asymmetric O-1*s* peak indicates the coexistence of various chemical bonds in the composite films. The peak at 531.2 eV (O_v) corresponds to O^{2-} in an oxygen deficient region [**32**]. The intensity of the 531.2 eV peak increases with increasing ZnO concentration. The high binding energy component of the O-1*s* peak at 532.5 eV (O_s) is characteristic for the presence of OH^- groups integrated in the material and to loosely bound oxygen on the surface such as H_2O [**33**]. Earlier, Sharma *et al.* [**34**] have assigned the 532.0 eV peak to absorbed hydroxyl ions in pure SnO_2 films prepared by spray technique. The film with 10 wt % and 50 wt % ZnO further shows one additional peak at 533.4 ± 0.3 which might be attributed to weakly bound surface oxygen (i.e. presence of O_2^{2-} anions) in the composite structures [**35**].

Fig. 6 summarizes the electrical resistivity results of as-deposited and annealed ZnO-SnO_2 binary-binary oxide thin films. The resistivity plot follows the same trend as the as-deposited ZnO-SnO_2 films, reported earlier [**26**]. Earlier Kilić and Zunger [**36**] have established that the activation energy for the formation of oxygen vacancies and tin interstitials in SnO_2 is quite low and accordingly these

Copyright © 2016 VBRI Press

defects can readily create. Finally, these defects tries to enhance the conductivity in doped (e.g., In-doped SnO_2) and non-stoichiometric SnO_2. The conglomeration of an extrinsic oxide like ZnO with SnO_2 in bulk amount further increases its charge carrier concentration, resulting in a reduction in the resistivity.

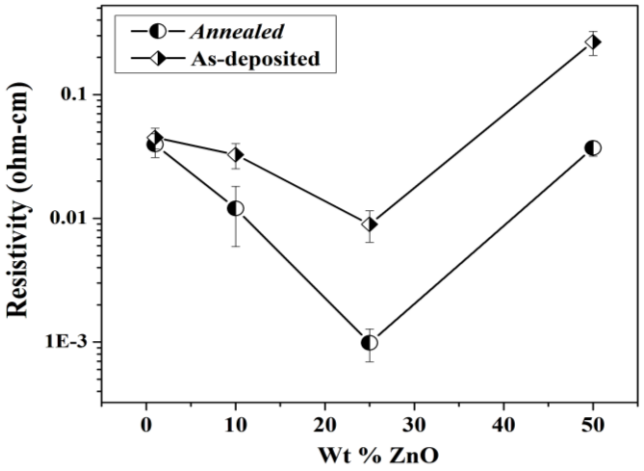

Fig. 6. Variations of electrical resistivity of as-deposited and annealed ZnO–SnO_2 thin films as a function of increasing ZnO concentration (plotted in logarithmic scale).

The resistivity of ZnO-SnO_2 films is consistently lower (follows a non-linear pattern) than that of the as-deposited films and reaches as low as ~9.84 x 10^{-4} Ω-cm (25 wt % ZnO film). This low resistivity may possibly be due to further increase in mobility and carrier concentration due to annealing at 600 °C in air. However, the relatively high resistivity in the film with 50 wt % ZnO is largely caused by the compositional variation and the existence of compositional and structural difference. It can be observed that the film with 50 wt % ZnO is the smoothest with lowest RMS roughness (RMS~8.62 nm), yielding maximum defects and strain variations, which would obstruct the flow of electrons and increases the resistivity. A comparative study reveals that the electrical resistivity of the annealed ZnO-SnO_2 films is an order of magnitude lower compared to its as-deposited counterpart. It may be presumed that due to thermal annealing there is a greater possibility of diffusion of Sn atoms from grain boundary and interstitial lattice sites to regular ZnO lattice sites [**37**]. Annealing influences the grain growth, subsequently resulting in less grain boundary area, which finally, reduces the grain-boundary scattering. The mobility of the charge carriers, therefore, enhances in the annealed films. Consequently the resistivity of the films decreases in of the ZnO-SnO_2 films in annealed state.

Conclusion

In summary, the structural, chemical and optical properties of post-annealed ZnO–SnO_2 (ZTO) thin films with varying concentrations have been studied. The ratios of zinc oxide to tin oxide were formulated to range from 1:99 to 50:50. It was observed that upon thermal annealing, the crystallinity of the composite films increases significantly with increasing concentration of ZnO compared to as-deposited state. The surface roughness of the films also decreases with increasing ZnO concentration. The average optical transmittance of the annealed ZTO films in the visible range (400-800 nm) decreases from 92 % to 78 % with increasing ZnO concentration in the film. It was found that by controlling the ZnO/SnO_2 ratio in the composite aggregate, the optical band gap of the PLD films could be finely tuned between the bandgap (E_g) of ZnO (E_g~3.37 eV) and SnO_2 (E_g~3.6 eV). The atomic ratios of the ZnO–SnO_2 composite films, as obtained from the XPS spectrum, confirms the formation of mixed oxides rather than alloyed phases. The XPS data revealed that in ZnO–SnO_2 films, Sn is present in Sn (+4) state, while Zn and O is present in mixed chemical states. The electrical resistivity of the annealed ZnO–SnO_2 films substantially decreased with increasing ZnO concentration and also compared to those of as-deposited films. The lowest resistivity (9.8 × 10^{-4} Ω cm) is obtained for the post-annealed film with 25 wt % ZnO. The reduction may be attributed to an increase in carrier concentration and mobility due to diffusion process, and less grain-boundary scattering. The present investigation shows that ZnO - SnO_2 binary-binary annealed films (with ≤ 25 wt% ZnO) could be a potential candidate for optoelectronic applications, such as solar cells or touch panel controls owing to their excellent structural, optical and electrical properties.

Acknowledgements

Partial financial supports from the Department of Science and Technology and Council of Scientific and Industrial Research (CSIR), Government of India are gratefully acknowledged. The author would gratefully acknowledge the DST-FIST funded XPS facility in the Department of Physics and Meteorology at IIT Kharagpur to perform the XPS measurements.

Reference

1. Kumar, M.; Wen, L.; Sahu. B. B.; Han , J. G. *Appl. Phys. Lett.* **2015**, *106*, 241903. **DOI**: 10.1063/1.4922732
2. Wen, L.; Kumar, M.; Sahu, B.B.; Jin, S.B.; Sawangrat, C.; Leksakul, K.; Han, J. G. *Surf. Coat. Technol.***2015**, *In Press*, **DOI:** 10.1016/j.surfcoat.2015.06.084
3. Sahu, B. B.; Han, J.G.; Kim, J.B.; Kumar, M.; Jin, S.; Hori M. *Plasma Process Polym.* **2015**, *in press.* **DOI:** 10.1002/ppap.201500094
4. Tian, Z.R.; Voigt, J.A.; Liu, J.; Mckenzie, B.; Mcdermott, M.J.; Rodriguez, M.A.; Konishi, H.; Xu, H. *Nat. Mater.* **2003**, *2*, 821. **DOI:** 10.1038/nmat1014
5. Zeng, H.; Duan, G.; Li, Y.; Yang, S.; Xu, X.; Cai W. *Adv. Funct. Mater.* **2010**, *20*, 561. **DOI:** 10.1002/adfm.200901884
6. Gedamu, D.; Paulowicz, I.; Kaps S.; Lupan, O.; Wille, S.; Haidarschin, G.; Mishra, Y. K.; Adelung, R. *Adv. Mater.***2014**, *26*, 1541. **DOI:** 10.1002/adma.201304363
7. Mishra, Y. K.; Kaps, S.; Schuchardt, A.; Paulowicz, I.; Jin, X.; Gedamu, D.; Freitag, S.; Maria Claus, M.; Wille, S.; Kovalev, A.; Gorb S.N.; Adelung, R. *Part Syst Charact.* **2013**, *30*, 775. **DOI:** 10.1002/ppsc.201300197
8. Jin , X. ; Strueben, J.; Heepe, L.; Kovalev, A.; Mishra, Y.K.; Adelung, R.; Gorb S.N.; Staubitz, A. *Adv. Mater.* **2012**, *24*, 5676. **DOI:** 10.1002/adma.201201780
9. Hirkac, V.; Kienle, L.; Kaps, S.; Lotnyk, A.; Mishra, Y.K.; Schürmann, U.; Duppel, V. ; Lotsch, B. V.; Adelung, R. *J. Appl. Cryst.***2013**, *46*, 396. **DOI:** 10.1107/S0021889812051333
10. Najim, M.; Gaurav Modi, Mishra, Y.K.; Adelung, R.; Singh, D.; Agarwala, V.; *Phys. Chem. Chem. Phys.*, **2015**, *17*, 22923. **DOI:** 10.1039/C5CP04293C

 Copyright © 2016 VBRI Press

11. H, Papavlassopoulos.; Mishra, Y.K.; Kaps, S.; Paulowicz, I.; Abdelaziz, R.; Elbahri, M .; Maser, E.; Adelung, R.; Röhl, C.; *PLoS ONE* , **2014**, *9*, e84983; **DOI:** 10.1371/journal.pone.0084983
12. Mishra, Y. K.; Chakravadhanula, V. S.K .; Hrkac, V.; Jebril, S.; Agarwal, D. C.; Mohapatra, S .; Avasthi, D. K .; Kienle, L .; Adelung R .*J. Appl. Phys.* **2012**, *112*, 064308. **DOI:** 10.1063/1.4752469
13. Mishra, Y.K.; Modi, G.; Cretu, V.; Postica, V.; Lupan, O.; Reimer, T.; Paulowicz, I.; Hrkac, V.; Benecke, W.; Kienle, L.; Adelung, R. *ACS Appl. Mater. Interfaces* **2015**, *7*, 14303. **DOI:** 10.1021/acsami.5b02816
14. Paulowicz, I.; Hrkac, V.; Kaps, S.; Cretu, V.; Lupan, O.; Tudor Braniste, T.; Duppel, V.;Tiginyanu, I.; Kienle, L.; Adelung R.; Mishra, Y. K. *Adv. Electron. Mater*. **2015**, *1*, 1500081; **DOI:** 10.1002/aelm.201500081
15. Lupana O.; Braniste, T.; Denga, M.; Ghimpuc, L.; Paulowicz , I.; Mishra, Y.K.; Kienle, L.; Adelung, R.; Tiginyanu, I. *Sens Actuators. B: Chem*, **2015**, *221*, 544. **DOI:** 10.1016/j.snb.2015.06.112
16. Chopra, K. L; Major, S.; Pandya, D. K. *Thin Solid Films*, **1983**, *1*, 102. **DOI:** 10.1016/0040-6090(83)90256-0
17. Kim, H; Pique´, A; Horwitz, J. S; Mattoussi, H; Murata, H.; Kafafi, Z. H ; Chrisey, D. B. *Appl. Phys. Lett.* **1999**, *74*, 3444. **DOI:** 10.1063/1.124122
18. Kim, H; Gilmore, C. M; Pique´, A; Horwitz, J. S; Mattoussi, H. Murata, H; Kafafi, Z. H; Chrisey, D. B. *J. Appl. Phys.* **1999**, *86*, 6451. **DOI:** 10.1063/1.371708
19. Tang, C. W; Van Slyke, S. A. *Appl. Phys. Lett.* **1987**, *51*, 913. **DOI:** 10.1063/1.98799
20. Minami, T. *Semicond. Sci. Technol*. **2005**, *20*, S35. **DOI:** 10.1088/0268-1242/20/4/004
21. Agura, H; Okinaka, H; Hoki, S; Aoki, T; Suzuki, A; Matsushita, T; Okuda, M. *Electr. Eng. Jpn*. **2005**,*151*, 40. **DOI:** 10.1002/eej.20026
22. Park, S. M, Ikegami, T; Ebihara, K.; *Thin Solid Films*. **2006**, *90*, 513. **DOI:** 10.1016/j.tsf.2006.01.051
23. Minami, T; *MRS Bull.***2000**, *25*, 38. **DOI:** 10.1557/mrs2000.149
24. Minami, T; Sonohara, H.; Takata, S; Sato, H. *Jpn. J. Appl. Phys.***1994**, *33*, L1693. **DOI:** 10.1143/JJAP.33.L1693
25. Chrisey, D. B; Hubler, G. K. Pulsed Laser Deposition of Thin Films; Wiley: New York, **1994**. **DOI:** 10.1039/A804929G
26. Sinha, S. K; Rakshit, T; Ray, S.K; Manna, I. *Appl. Surf. Sci*. **2011**, *257*, 10551. **DOI:** 10.1016/j.apsusc.2011.07.049
27. Peiteado, M; Iglesias., Y.; Frutos, J. D.; Fernandez, J. F.; Caballero, A. C.; *Bol. Soc. Esp. Ceram. V.* **2006**, 45,158. **DOI:** 10.1016/j.sna.2006.05.031
28. Cook, L. P.; McMurdie, H. F.; Ondik, H. M., Phase Diagrams for Ceramists. Volume VII, The American Ceramic Society, Inc., Westerville, Ohio, **1989**. **DOI:** 10.1016/1989.12.001
29. Young, D. L; Ph.D. Thesis, Colorado School of Mines, **2000**. **DOI:** 10.1005/2000.15.105
30. Tauc, J.; Grigorovici, R.; Vancu, A. *Phys. Status Solidi B.* **1966**, *15*, 627. **DOI:** 10.1002/pssb.19660150224
31. Young, D.L.;Moutinho, H.; Yan, Y.; Coutts, T. J. *J. Appl. Phys.* **2002**, *92*, 310. **DOI:** 10.1063/1.1483104
32. Fan, J. C.; Goodenough, J. B. *J. Appl. Phys.* **1977**, *48*, 3524. **DOI:** 10.1016/0040-1977(1) 9095
33. Dupin, J.C. ; Gonbeau, D. ; Vinatier, P. ; Levasseur, A. *Phys. Chem. Chem. Phys*.**2000**, *2*, 1319. **DOI:** 10.1039/A908800
34. Sharma, D. D.; Hegde, M.S.; Rao, C. N. R. *J. Chem. Soc. Faraday Trans*. II , **1981**, *77*, 1509. **DOI:** 10.1039/F29817701509
35. Ghuang, T.J.; Brundle, C.R.; Rice, D. W. *Surf. Sci.* **1979**, *59*, 413. **DOI:** 10.1007/1035/1979.2.57
36. Kiliç, C.; Zunger, A. *Phys. Rev. Lett*. **2002**, *88*, 095501. **DOI:** 10.1103/PhysRevLett.88.095501
37. Wu, W. F.; Chiou, B. S. *Appl. Surf. Sci.* **1993**, *68*, 497. **DOI:** 10.1016/0169-4332(93)90233-2

.

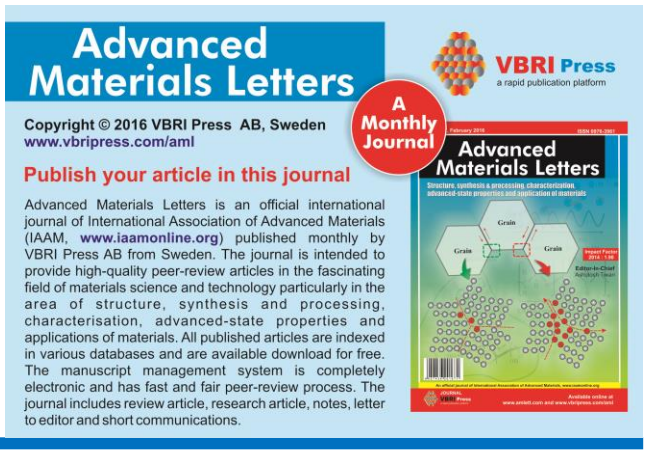

 Copyright © 2016 VBRI Press